NUMERICAL INVESTIGATIONS OF COOLING HEAT TRANSFER OF SUPERCRITICAL WATER

H. Herbell[1], J. Starflinger[2] and T. Schulenberg[3]
[1] EnBW Kernkraft GmbH, Kernkraftwerk Philippsburg, Germany
[2] IKE, University of Stuttgart, Germany
[3] Karlsruhe Institute of Technology, Karlsruhe, Germany

Abstract

The re-heater and the start-up system are the only basically new components in the balance of plant of the High Performance Light Water Reactor (HPLWR). Inside the tubes of the re-heater, supercritical fluid undergoes pseudo-condensing. CFD simulations have been performed in order to determine the heat transfer coefficient on the tube side more accurately. Numerical results are compared with Bruch's CO_2-experiment [12] for validation. The results illustrate the influence of buoyancy forces on the laminar turbulent transition for vertical downward flows. A simple heat transfer correlation [17] has been proposed for re-heater design, which is compared here with numerical simulations. Fluctuating density stratification is obtained for a horizontal layout which is similar to a Kelvin-Helmholtz instability.

1. Introduction

In the High Performance Light Water Reactor (HPLWR), the coolant is heated to temperatures as high as 500°C at 25 MPa system pressure and delivered to a once through steam cycle. A thermal power of 2300 MW is used to heat a mass flow rate of 1179 kg/s from 280°C reactor inlet temperature. The HPLWR reaches a net efficiency of 43.5% with a net output of 1000 MW_{el}. The three pass core design [1] uses intermediate mixing after each heat-up step to homogenize the temperature distributions, and to avoid peak cladding temperatures beyond feasible material limits. The steam cycle adopts technology from supercritical fossil fired power plants (FFPP) and currently operated boiling water reactors (BWR). The conversion cycle includes a seven stage pre-heater setup [2] and a non speed reduced turbine generator train with high, intermediate, and low pressure (HP, IP and LP) units [3]. Besides the start-up system, the re-heater is the only new component in the HPLWR balance of plant. However, it utilizes BWR and FFPP technologies as well.

Like with FFPP, a typical BWR includes a regenerative re-heating lowering the amount of moisture in the last LP turbine stages to avoid excessive erosion-corrosion. Compared with FFPP, however, the upper pressure level is significantly lower in BWR (7.8 MPa). Thus, the BWR balance of plant system configuration consists only of two turbine sub-sections called HP and LP turbine. In addition, the re-heater of a BWR needs a moisture separator. Hot steam extracted directly after the reactor is used to heat steam released from HP turbine. Energy at high temperatures is transferred to lower temperatures in the regenerative re-heater, which means a waste of exergy. On the other hand, a small net efficiency gain is usually provided due to increased turbine efficiency because of higher exit quality of the LP turbine [4]. Oka et al. [5] adopted this concept of re-heating for the Super LWR and placed a moisture separator re-heater between IP and LP turbine.

In FFPP, re-heating is a conventional method to increase the efficiency and the specific turbine power. After the HP turbine, the released steam is heated with the hot exhaust gas before entering the IP turbine. There is no need for water separation. In analogy, Bitterman et al. [6] adopted this re-heat concept for the HPLWR project by placing a reheater after the HP turbine. This concept excels in simplification because a water separator can be omitted. IP pressure fuel assemblies are avoided in the reactor as well by using steam extracted directly after the reactor.

Both re-heating concepts of Supercritical Water Cooled Reactors (SCWR) include a tube and shell heat exchanger with pseudo-condensing supercritical steam inside the tubes, i.e. change of enthalpy from superheated to sub-cooled conditions, while saturated or slightly superheated steam is reheated outside. The cooling process includes a high density change (from 80 kg/m³ to 582 kg/m³ for the HPLWR) without phase change of the supercritical fluid. In this paper, the accurate determination of cooling heat transfer of supercritical fluids is investigated. The influence of buoyancy forces on the flow profile is examined numerically. Moreover, stability and density stratification are considered for a cooled horizontal tube with supercritical water.

2. Heat transfer of supercritical fluids

The heat transfer process with supercritical fluids under heating conditions has been the focus of intensive research in the last decades. Pioro and Duffey [7] give a literature review on the heat transfer behaviour of supercritical fluids. Together with numerical investigations, it can be concluded that the heat transfer coefficient of supercritical fluid flows is strongly affected by heat flux and flow direction. Four different heat transfer regimes have been specified [8]:

- Enhanced heat transfer
- Transitional region: the peak in heat transfer coefficient near the pseudo-critical point decreases, however the wall temperature rise is still negligible
- A property variation, e.g. thermal conductivity, in the near wall layer which leads to heat transfer deterioration because of a thin vapour-like insulating layer in the vicinity of the heated wall
- Buoyancy induced heat transfer deterioration with significant reduction of turbulent intensity and re-laminarisation of the flow, typically M-shaped velocity profiles

In contrast to heating, the cooling process has not been investigated to similar extend. Dang and Hihara investigated experimentally [9] and numerically [10] the heat transfer coefficient of supercritical carbon dioxide (SCO_2) cooled in horizontal tubes with inner diameters ranging from 1 to 6 mm. They developed a modified Gnielinksi equation by selecting the reference temperature accurately. The experimenters report difficulties in interpreting the results because of radial distributions of the thermo-physical properties. Additionally, they tested several turbulence models and proposed a low Reynolds number k-ε model for best matching. Kruizenga et al. [11] performed heat transfer experiments with SCO_2 in a semi circular test section. They compared experimental and numerical results with several Nusselt number correlations and revealed that the heat transfer coefficient is over predicted at the pseudo-critical temperature by all tested correlations compared to the experimental determined values. Furthermore, they found a good agreement between the experiments and the numerical simulations if the enhanced wall treatment is used with either the k-ε or the SST k-ω model.

Bruch et al. [12] added an experimental investigation of cooled SCO_2 in vertical downward and upward flow. The influence of flow direction and thus buoyancy force has been examined by comparing the heat transfer coefficients for upward and downward flow. This experiment is chosen now to validate a CFD approach investigating heat transfer and buoyancy effects for the HPLWR re-heater.

3. Experimental apparatus

The experimental test loop of Bruch [12] consists of two vertical tube-in-tube heat-exchangers connected in series by means of a U-bend. In the following, only the sub-section for vertical downward flow is considered. Each sub-section is 0.75m long, and SCO_2 is flowing in the inner copper tube of 6 mm inner diameter. Cooling water flows in the annulus around. The SCO_2 mass flow rate is determined using a Coriolis mass flow meter. Absolute pressure is measured before the test section and differential pressure after the test section. Bulk temperatures are measured before and after the cooled length.

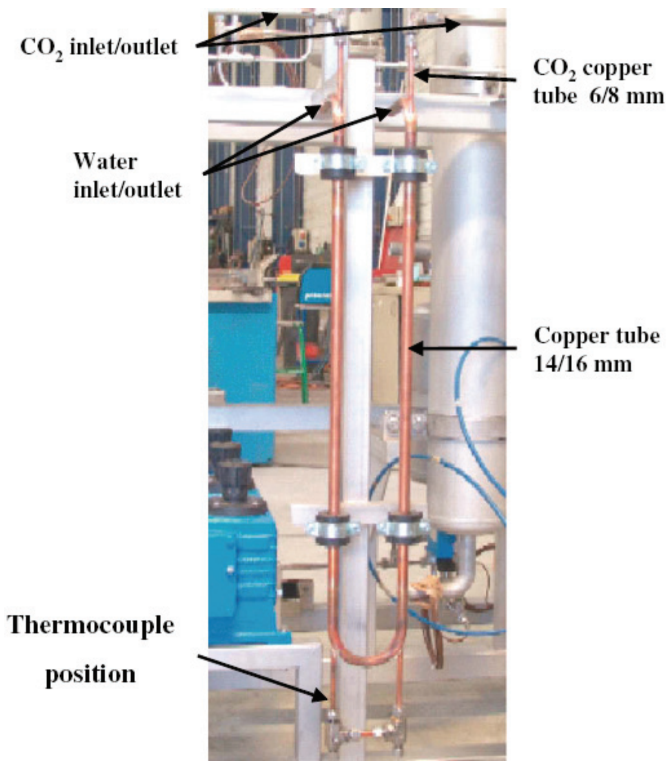

Figure 1 Experimental test facility of Bruch [12]: tube in tube test section

An integral method has been used by Bruch et al. [12] to determine the heat transfer coefficient of the SCO_2 to the heat exchanger wall. The transferred heat of the SCO_2 can be determined with the measured mass flow rate $\dot{m}$ and the enthalpy difference of the cooled SCO_2 $(dh)_{CO_2}$.

$$d\dot{Q} = \dot{m} \cdot (dh)_{CO_2} \tag{1}$$

Now integral temperatures are introduced for the cooling water and the cooled SCO_2:

$$\overline{T}_{Water} = \frac{T_{Water,out} + T_{Water,in}}{2} \text{ and } \overline{T}_{CO_2} = \frac{T_{CO_2,out} + T_{CO_2,in}}{2} \tag{2}$$

For all investigated experimental test runs the cooling water temperature difference was below 0.25K. The temperature difference for the supercritical SCO_2 was in the range of 1.5K to 4.7K. The overall integral heat transfer coefficient k could be determined as:

$$\dot{Q} = k \cdot A \cdot (\overline{T}_{Water} - \overline{T}_{CO_2}) \tag{3}$$

The heat transfer coefficient on the SCO_2 side was calculated from the overall heat transfer coefficient as shown below:

$$\frac{1}{k} = \frac{1}{\alpha_{CO_2}} + \frac{A_{in}}{A_{out} \cdot \alpha_{Water}} + \frac{A_{in}}{2 \cdot \pi \cdot \lambda_w \cdot L} \cdot \ln\left(\frac{D_{in}}{D_{out}}\right) \tag{4}$$

The heat transfer coefficient on the water side was calculated using the Dittus and Boelter [13] correlation. The thermal conductivity of the wall was assumed to 300 W/(m²K).

4. Computational approach

In order to simulate the experiment described above, a CFD approach is applied here. The commercial CFD package STAR-CD 3.26 is used to solve the Reynolds-averaged Navier-Stokes equations together with the equation for transport of turbulent kinetic energy and the turbulent frequency, resp. turbulent energy dissipation. The Shear Stress Transport (SST) [14] turbulence model with enhanced wall treatment is used, similar to those simulations previously performed by other researchers [15], [16] for heated supercritical fluids. The non-dimensional distance of the first computational node from the wall (y^+) is kept below 1, in order to resolve the boundary layer properly. The computational domain consists of the complete length of the inner tube, but the tube wall is not modelled. The inlet velocity and the outlet pressure serve as boundary conditions. The average bulk temperature of the cooling water and the resistance from the coolant to and through the heat exchanger wall are fixed as boundary conditions on the fluid domain border in order to have realistic boundary conditions. The thermal-physical properties of SCO_2 at constant pressure are implemented as functions with a user coding. Buoyancy effects are taken into consideration, according to variable density with temperature differences.

4.1 Comparison of numerical simulations with experimental data

Figure 2 depicts a comparison of the numerical simulations with the experimental data [12]. Every single data point represents a steady-state experimental measurement. The experiments have been performed with vertical downward flow for a pressure of 8 MPa and a mass flux of 200 kg/(sm²). The average heat transfer coefficient is plotted over the mean bulk temperature. The integral heat transfer coefficient, derived from the CFD simulations, is determined in the same way as described above for the experimental results [12]. Additionally, the local heat transfer coefficient is shown, which has been calculated with the local heat flux and local wall temperature at the half axial length of the test section. The local heat transfer coefficient is plotted over the local values of the bulk temperature.

Experimental results and numerical calculations agree reasonable well in the gas-like region and in the pseudo-critical region. Local and integral methods of determining the heat transfer coefficient show acceptable deviations in the vicinity of the pseudo-critical point: 9% deviation for the integral method and 22% for the local method. However, large differences between the CFD simulations and the experiments [12] are obtained in the liquid-like region. The predicted heat transfer coefficient is more than four times higher than the experimental data for the experiment with lowest temperature. It has to be noted that bulk temperatures and wall temperatures are below the pseudo-critical temperature at the inlet and at the outlet of the test section for the three experimental measurements on the left hand side. Contrary to the experiments [12], the CFD simulations predict a reasonable value for the heat transfer coefficient for turbulent flow.

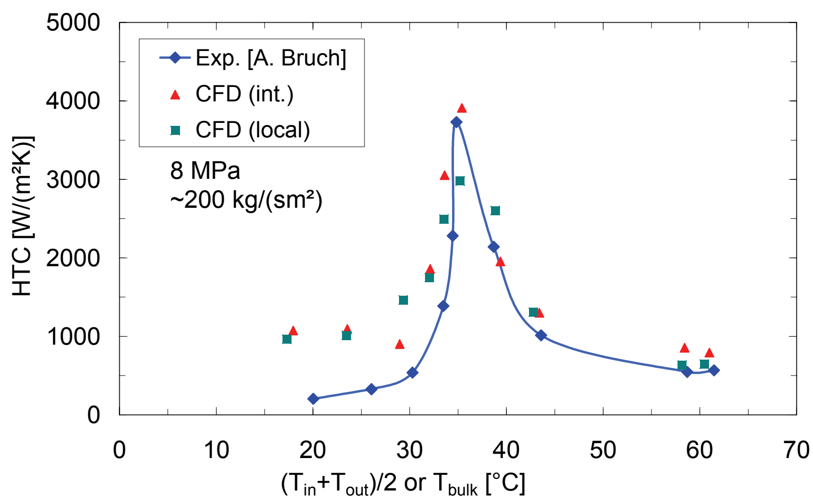

Figure 2 Comparison of experimental data with CFD simulations: local and integral method of determining the heat transfer coefficient (HTC), CO_2, 8 MPa, 200 kg/(sm²)

4.2 Turbulence influence

The Reynolds number is increasing with each test run for higher bulk temperatures (from left hand side to right hand side). In the liquid like region, Reynolds numbers are in the range from 15,000 to 20,000. For comparison, laminar simulations have been performed for the three test runs with lowest bulk temperatures. Now, excellent agreement could be achieved for the test run with lowest bulk temperature (deviation <5%), cp Figure 3. For this test run, the Reynolds number was lowest. With increasing bulk temperature and increasing Reynolds number, the laminar CFD simulations underestimate the experimental data, indicating a transition from laminar to turbulent flow.

Figure 4 depicts the velocity profiles of the turbulent and the laminar simulations with 20°C bulk temperature at the half axial length of the test section. The temperature drop in this experiment was only 1.5 K, thus the heat transfer coefficient is not changing significantly along the heated length. The turbulent simulations reveal a flat velocity profile. The gravity has only minor influence on the results. In contrast, the laminar simulations exhibit a M-shape velocity profile, which could influence the laminar turbulent transition. A fourth velocity profile is plotted for laminar flow without buoyancy influence for verification. This velocity profile shows the typical parabolic shape for laminar flow.

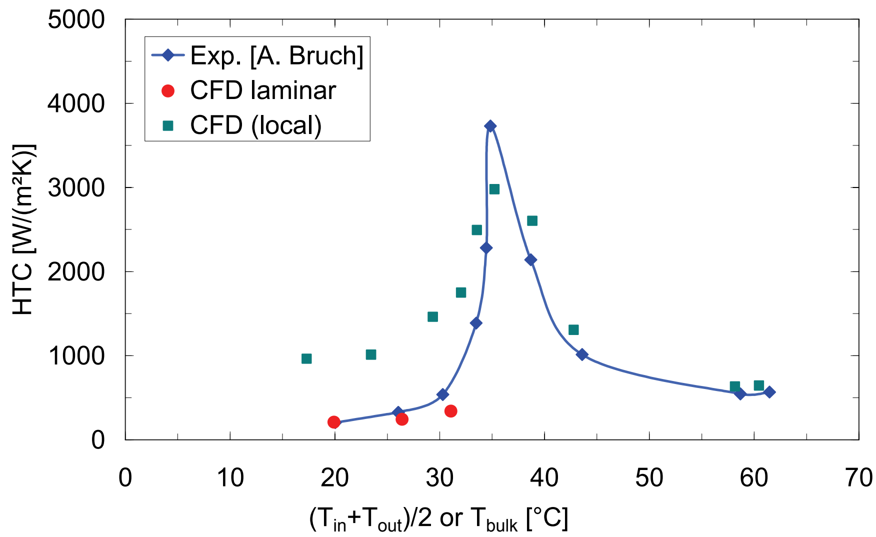

Figure 3 Comparison of experimental data [12] with CFD simulations: laminar and turbulent simulations, CO_2, 8 MPa, 200 kg/(sm²)

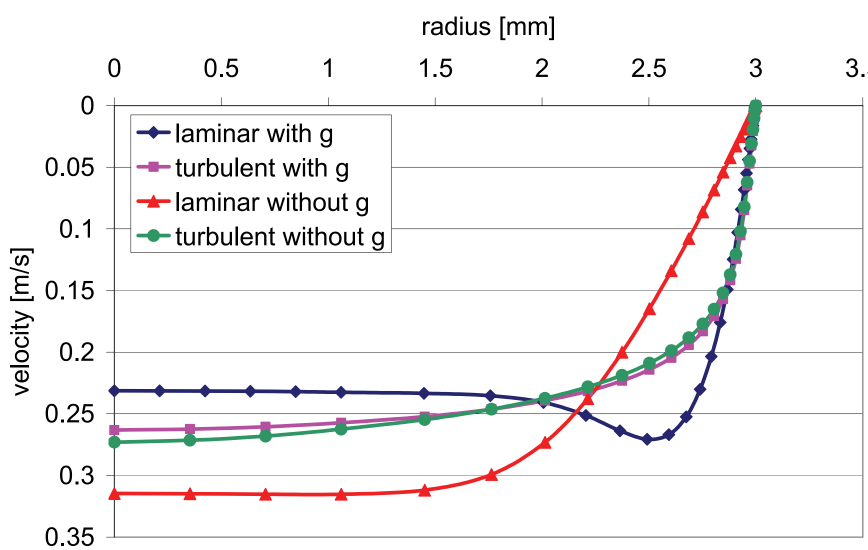

Figure 4 Velocity profiles for turbulent and laminar simulations, with and without buoyancy force for 20°C bulk temperature, at the half axial length of the test section, CO_2, 8 MPa, 200 kg/(sm²)

4.3 Comparison of experimental data with selected heat transfer correlations

Bruch et al. [12] proposed a modified Jackson and Hall heat transfer correlation for turbulent flow to match the experimental data, because the Reynolds number given is a value that indicates turbulent flow. In Figure 5 the original Jackson and Hall [17] correlation is plotted and compared with the experimental data [12]. Large differences between the prediction models and the experimental data are noted, in particular in the liquid-like region. Instead of introducing a factor to match the experimental results, the data of the Bruch's experiment is compared here with several turbulent and laminar heat transfer correlations. The heat transfer correlations for turbulent flow have the general form of a modified Dittus and Boelter [13] equation:

$$Nu = C \cdot \mathrm{Re}^n \cdot \mathrm{Pr}^m \cdot F \tag{5}$$

This correlation uses only bulk temperature and its fluid properties. Jackson and Hall [17] heat transfer correlation is more sophisticated including wall temperature depending fluid properties. Additionally, a simple heat transfer correlation, proposed by Cheng et al. [18] shall be compared with the CFD simulations to determine the heat transfer of SCO_2 under cooling conditions. Therein a correction F has been introduced based on the Dittus and Boelter correlation [13]. This correction factor is defined by the acceleration number π_A which includes the thermal expansion coefficient β, the specific heat capacity c_p, heat flux q and mass flux G. The subscript $\pi_{A,PC}$ means material properties and conditions at the pseudo-critical point.

$$\pi_A = \frac{\beta}{c_p} \cdot \frac{q}{G}. \tag{6}$$

Good agreement could already be achieved for this heat transfer correlation in comparison with several deteriorated heat transfer experiments for heating conditions [18]. Table 1 summarized the selected correlations of heat transfer coefficient.

	C	n	M	F
Dittus-Boelter [13]	0,023	0,8	0,33	1,0
Jackson and Hall [19]	0,0183	0,82	0,5	$\left(\frac{\rho_w}{\rho_b}\right)^{0,3}$
Cheng [17]	0,023	0,8	0,33	$F = \min(F_1, F_2)$, $F_1 = 0,85 + 0,766 \cdot (\pi_A \cdot 10^3)^{2,4}$, $F_2 = \frac{0,48}{(\pi_{A,PC} \cdot 10^3)^{1,55}} + 1,21 \cdot \left(1 - \frac{\pi_A}{\pi_{A,PC}}\right)$

Table 1 Selected heat transfer correlations for turbulent flow

Additionally, two heat transfer correlations for buoyancy affected laminar flow are introduced: Jackson et al. [19] and Behzadmehr [20] are based on the quotient of Grashof and Reynolds number.

$$Nu = 0,95 \cdot (Gr / \mathrm{Re})^{0,28} \tag{7}$$

$$Nu = 4,36 \cdot \left(1 + \frac{Gr^{0,468}}{750 + 0,24 \cdot \mathrm{Re}}\right) \tag{8}$$

In figure 5 the selected heat transfer correlations for turbulent flow and both heat transfer correlations for buoyancy affected laminar flow are compared with Bruch's experiment [12]. The first three test runs with lowest temperatures are in good agreement with the experimental data indicating laminar flow. All heat transfer correlations for turbulent flow over predict the experimental results. The fourth test run (from the left hand side) is between the laminar and the turbulent heat transfer correlations, indicating a transitional region between laminar and turbulent flow. The last six test runs (from right hand side) are in reasonable agreement with the turbulent simulations. It deserves mentioning that the Dittus and Boelter [13] heat transfer correlation has best matching with the experimental data. X.Cheng [18] and Jackson and Hall [17] heat transfer correlation over predict the heat transfer coefficient in the vicinity of the pseudo-critical point.

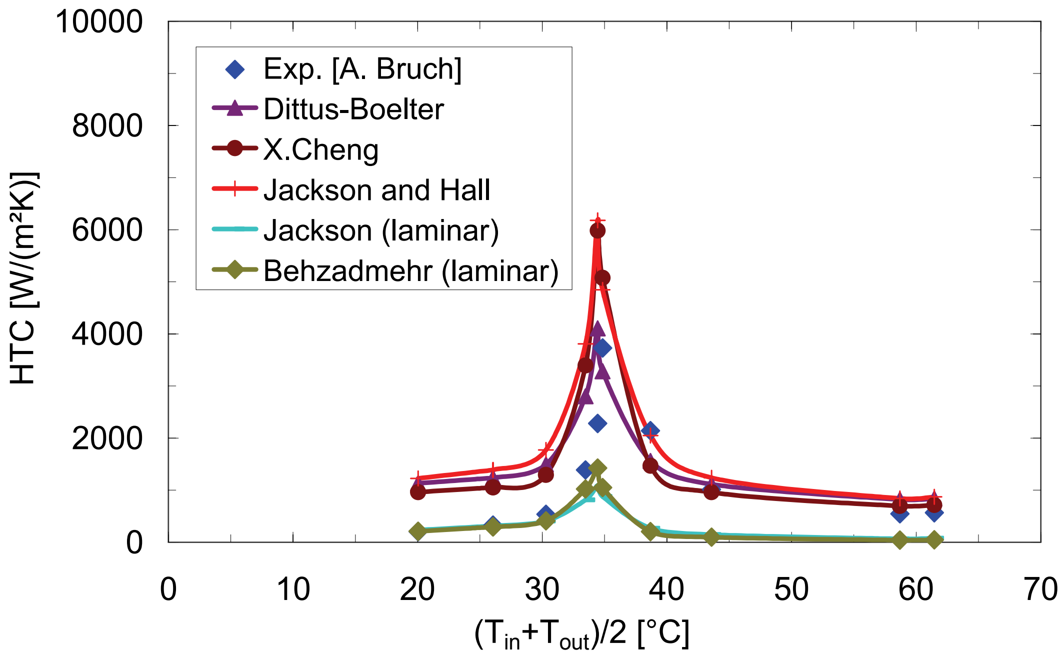

Figure 5 Comparison of experimental data [12] with selected heat transfer correlations for laminar and turbulent flow, CO_2, 8 MPa, 200 kg/(sm²)

4.4 Heat transfer prediction for the HPLWR re-heater

The HPLWR re-heater proposed here consists of a tube bundle with 15 m length and each tube has an inner diameter of 12 mm. Inside the tubes, supercritical water undergoes pseudo-condensing, whereas the shell side is superheating intermediate pressure steam. The arrangement is assumed to be vertical and the supercritical fluid enters the re-heater from top and leaves it from bottom. As mentioned before, buoyancy forces could lead to turbulence damping. However, laminar heat transfer coefficients, as predicted in the experiment of Bruch [12], are not to be expected because of higher Reynolds numbers (50,000 at inlet and 20,000 at exit of the HPLWR re-heater tube). The Dittus and Boelter [13] heat transfer correlation is proposed here to predict the heat transfer coefficient for the cooled supercritical water accurately.

5. Buoyancy effects in a horizontal tube

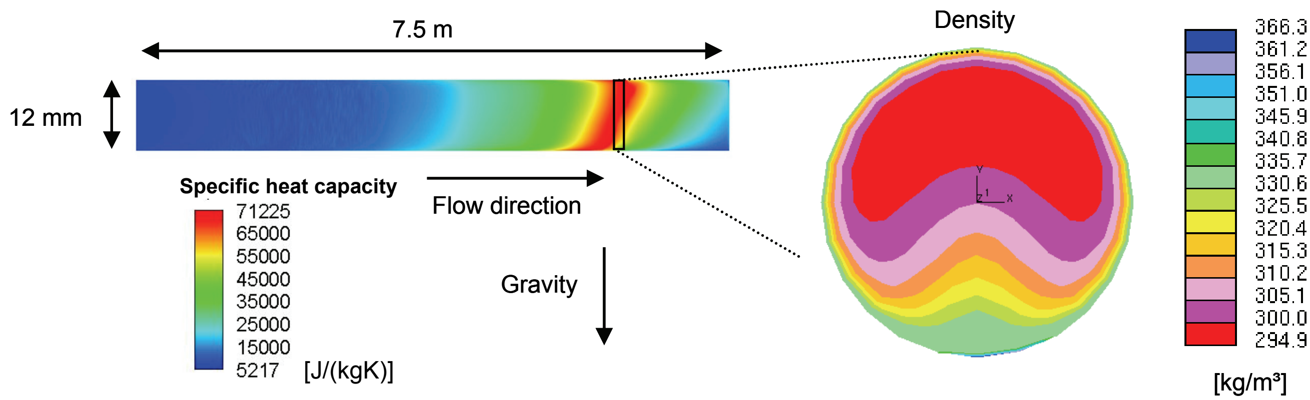

Figure 6 Horizontal layout of the HPLWR re-heater; left hand side: specific heat capacity along the second half of the axial length of the HPLWR re-heater tube; right hand side: density profile in the cross section at the pseudo-critical point, H_20, 25 MPa, 127 kg/(m²s).

The CFD simulations of Bruch's experiment [12] reveal that buoyancy forces are having a big influence on cooling heat transfer in vertical tubes. In general, vertical and horizontal layouts for the re-heater can be seen in currently operated nuclear power stations. Therefore, in order to provide future options, a horizontal layout has also been investigated. Hence, CFD-simulations of the heat transfer have been performed for a horizontal layout as well. Figure 6 depicts on the left hand side the second half length of one heat exchanger tube. The characteristic of the specific heat is plotted for the axial cross section of the tube. Due to the influence of buoyancy, stratification can be expected. This effect becomes more obvious if the density is evaluated. On the right hand side of Figure 6, the density characteristic is shown for the tube cross section. The density equals 317.22 kg/m³ at the pseudo-critical point of water (for 25 MPa and 384.87°C). In one cell layer, densities higher and lower than the density at the pseudo-critical point can be seen. The influence of buoyancy is identified in the profile of the stratification. The pseudo-critical fluid pseudo-condenses on the wall and fluid with higher density is collected at the bottom of the tube.

5.1 Unsteady CFD simulations

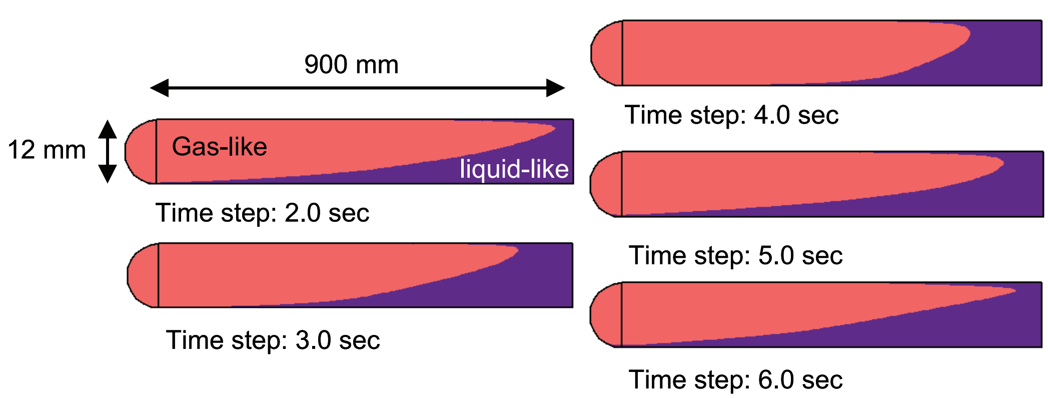

Figure 7 Density stratification in a horizontal HPLWR re-heater tube, 25 MPa, pseudo-critical temperature: 384.87°C, 317.22 kg/m³; gas-like densities pigmented with light colour, liquid-like densities pigmented with dark colour, H_20, 25 MPa, 127 kg/(m²s).

Unsteady CFD simulations have been performed to investigate the influence of buoyancy. The time step has been adjusted by the Courant criterion and equals 0.001 seconds. Figure 7 depicts a cut-out of one heat exchanger tube. Five time steps are shown from 2.0 to 6.0 seconds with an increment of 1.0 sec. Gas-like densities, e.g. densities below the density of the pseudo-critical point (317.22 kg/m³) are pigmented with light colour and liquid like densities, e.g. densities above 317.22 kg/s are pigmented with dark colour. The density stratification is not stable: position and shape of the gas-like layer are changing with time indicating waves at the liquid-gas-like interface. The heat transfer coefficient on top of the tube differs from the heat transfer coefficient on bottom. However the overall heat transfer is not changing with time.

5.2 Comparison of numerical results with Kelvin-Helmholtz instability criterion for two-phase flow

Instabilities in interfaces of two-phase flow with different densities ρ_1 and ρ_2 and velocities U_1 and U_2 are well-known as Kelvin-Helmholtz instabilities. Mathematical treatment results in the following correlation for the onset of instabilities [21]. Amplification of a surface disturbance is obtained when

$$g \cdot \left(\rho_2^2 - \rho_1^2\right) < a \cdot \rho_1 \cdot \rho_2 \cdot \left(U_1 - U_2\right)^2 . \tag{9}$$

The density and velocity differences of the supercritical water are approximated from time step 2.0 sec as depicted in Figure 8. A minimal wave number a can be calculated and a minimal wave length λ is obtained which is in the range of the simulated density fluctuations:

$$a = 60.2 \text{ and } \lambda > 0.1m . \tag{10}$$

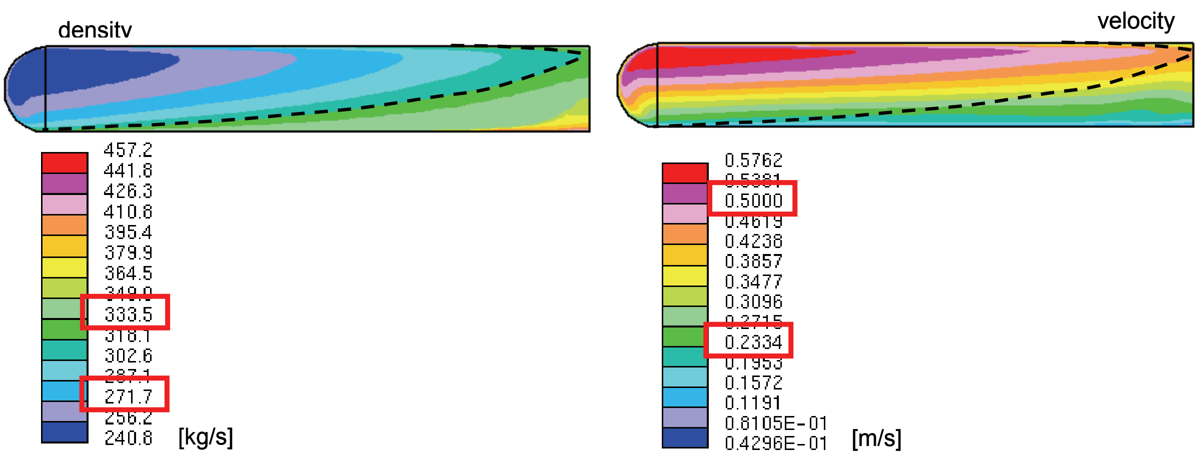

Figure 8 Density stratification: comparison with Kelvin Helmholtz instability criterion for time step 2.0 sec., H_20, 25 MPa, 127 kg/(m²s).

6. Conclusions

Numerical investigations of cooling heat transfer of supercritical fluids have been performed resulting in the following conclusion:

- Simulations of the Bruch's experiment [12] with vertical downward flow reveal buoyancy influences on cooling heat transfer. M-shaped velocity profiles influence the laminar turbulent transition of the flow. Up to a Reynolds number of 20,000, laminar heat transfer coefficients are observed in the experiment. Numerical simulations and experimental results agree reasonable well for the non-deteriorated test runs using the CFD approach recommended for heating. The deteriorated test runs are in good agreement with the laminar simulations. Selected laminar and turbulent heat transfer correlations are compared with the experimental data [12] resulting in an equivalent conclusion: the first three test runs can be predicted with correlations for buoyancy influenced laminar flow and test runs with Reynolds numbers above 20,000 are in good agreement with correlations for turbulent flow.

- Laminar heat transfer is not to be expected for the HPLWR re-heater because Reynolds numbers are in a higher range. Dittus and Boelter correlation is proposed here to predict the heat transfer of turbulent cooled flow with supercritical water.

- Numerical simulations of a horizontal arrangement of the HPLWR re-heater reveal density stratification due to buoyancy forces. Unsteady CFD simulations show fluctuating density waves which are similar to a Kelvin-Helmholtz instability. The heat transfer coefficient is not affected by the density fluctuations.

7. Acknowledgements

The authors gratefully acknowledge financial support by EnBW Kernkraft GmbH.

8. Nomenclature

A	Area, m²	Pr	Prandtl number, -
a	Wave number, 1/m	π_A	Acceleration number, defined in Eq. (9)
α	Heat transfer coefficient, W/(m²K)	$\dot{Q}$	Heat flow rate, W
β	Thermal expansion coefficient, 1/K	q	Heat flux, W/m²
c_p	Specific heat, J/(kgK)	Re	Reynolds number, -
D	Diameter, m	ρ	Density, kg/m³
F	Correction factor, -	$T,\overline{T}$	Temperature, average temperature °C, K
G	Mass flux, kg/(m²s)	U	Velocity, m/s
g	Acceleration of gravity, m²/s		
Gr	Grashof number, -		
h	Specific enthalpy, J/kg	Subscritps	
k	Overall heat transfer coefficient, W/(m²K)	CO_2	Refers to carbon dioxide
L	Length, m	*Water*	Refers to water
λ	Thermal conductivity, W/(mK)	*in*	Inlet, inner tube side
m	Coefficient, -	*out*	Outlet, outer tube side
n	Coefficient, -	*w*	Wall
Nu	Nusselt number, -	*pc*	Pseudo-critical

9. References

[1] T. Schulenberg, J. Starflinger, J. Heinecke, "Three pass core design proposal for a high performance light water reactor", Proceedings of the 2nd COE-INES-2 International Conference on Innovative Nuclear Energy Systems, Yokohama, Japan, 2006 Nov. 26-30

[2] M. Brandauer, M. Schlagenhaufer, T. Schulenberg, "Steam cycle optimization for the HPLWR", Proceedings of the 4th International Symposium on Supercritical Water-Cooled Reactors, Heidelberg, Germany, 2009 March 8-11

[3] H. Herbell, M. Wechsung, T. Schulenberg, "A turbine design concept for the high performance light water reactor", Proceedings of the 4th International Symposium on Supercritical Water-Cooled Reactors, Heidelberg, Germany, 2009 March 8-11

[4] F. G. Baily, E. H. Miller, "Modern turbine designs for water cooled reactors", *Nucl. Eng.* 12, 1967, p. 29-32

[5] Y. Oka, S. Koshizuka, Y. Ishiwatari, A. Yamaji, "Super light water reactors and super fast reactors", Springer Science+Business Media, 2010, pp. 230-232

[6] D. Bittermann, J. Starflinger, T. Schulenberg, "Turbine technologies for high performance light water reactors", Proceedings of the International Conference on Advances in Nuclear Power Plants, Pittsburgh, PA USA, 2004 June 13-17

[7] I.L. Pioro, R.B. Duffey, "Heat transfer and hydraulic resistance at supercritical pressures in power engineering applications", ASME Press, New York, NY, USA, 2007

[8] D. Palka, H. Anglart, "Investigations of the onset of heat transfer deterioration to supercritical water", Proceedings of the 4th International Symposium on Supercritical Water-Cooled Reactors, Heidelberg, Germany, 2009 March 8-11

[9] C. Dang, E. Hihara, "In-tube cooling heat transfer of supercritical carbon dioxide. Part 1. Experimental measurement", *Int. Journal of Refrigeration*, Vol. 27, 2004, pp. 736-747

[10] C. Dang, E. Hihara, "In-tube cooling heat transfer of supercritical carbon dioxide. Part 2. Comparison of numerical calculations with different turbulence models", *Int. Journal of Refrigeration*, Vol. 27, 2004, pp. 748-760

[11] A. Kruizenga, H. Li, M. Anderson, M. Corradini, "Investigations of heat transfer behaviour in turbulent, horizontal flows near the critical pressure", Proceedings of the technical meeting on heat transfer, thermal-hydraulics and system design for super-critical water-cooled reactors, Pisa, Italy, 2010, July 5-8

[12] A. Bruch, A. Bontemps, S. Colasson, "Experimental investigations of heat transfer of supercritical carbon dioxide flowing in a cooled vertical pipe", *International Journal of Heat and Mass Transfer*, 52, 2009, pp.2589-2598

[13] F.W Dittus., L.M.K. Boelter, "Heat Transfer in automobile radiators of the turbular type", Univ. Calif. Publ. Eng., Vol. 2, 1930, pp. 433-461

[14] F.R. Menter, "Two-Equation Eddy-Viscosity Turbulence Models for Engineering Applications", *AIAAJournal*, Vol. 32, Iss. 8, 1994, pp. 1598-1605

[15] D. Palko, H. Anglart, "Numerical study of heat transfer deterioration", Proceedings of the International Workshop on High Performance Light Water Reactors, Karlsruhe, Germany, 2008, March 31 to April 3

[16] Y. Zhe, E. Laurien, "Prediction of heat transfer of upward flow in annular channel at supercritical pressure – water and CO_2", Proceedings of the 4th International Symposium on Supercritical Water-Cooled Reactors, Heidelberg, Germany, 2009 March 8-11

[17] X. Cheng, Y.H. Yang, S.F. Huang, "A simplified method for heat transfer predication of supercritical fluids in circular tubes", *Annals of Nuclear Energy*, Vol. 36, 2009, pp. 1120-1128

[18] H. Oertel, "Prandtl's Essentials of Fluid Mechanics", Springer Verlag, New York, USA, 2004, pp. 419-422

[19] J.D. Jackson, W.B Hall, "Forced convection heat transfer to fluids at supercritical pressures", in: Turbulent Forced Convection in Channels and Bundles, Hemisphere, vol. 2, New York, 1979, pp. 563-611

[20] J.D. Jackson, M.A Cotton., B.P. Axcell, "Studies of mixed convection in vertical tubes", *International Journal of Heat and Fluid Flow*, Vol. 10(1), 1989, pp. 2-15,

[21] A. Behzadmehr, N. Galanis, A. Laneville, "Low reynolds number mixed convection in vertical tubes with uniform wall heat flux, *International Journal of Heat and Mass Transfer*, 46(25), 2003, pp. 4823-4835